CHAPTER III

THEORETICAL ASPECTES AND TECHNIQUE OF SOLAR FLUX DISTRIBUTION CALCULATION

In this chapter, we will discuss about the theoretical background needed for our work. First, sun position is defined by two angles, sun altitude and sun azimuth angle. Second, the mirror orientation of the central receiver system is calculated as a function of location and time. Finally, we will calculate the solar flux distribution using the superposition technique.

3.1 Solar Motion

To understand the trajectory of the sun, the relationship between the earth's axis of rotation and the plane of its orbit, the ecliptic has to be defined. The earth's axis makes an angle of about 23.5 degree to the normal vector of the plane. Figure 3.1 shows this relationship.

The intersection of the equatorial plane of the earth with the celestial sphere is called the celestial equator. The motion of the earth about the sun shown in Figure 3.1 is represented on the celestial sphere of Figure 3.2 by a circular orbit, called the ecliptic, which is tilted at approximately 23.5 degree with respect to the celestial equator.

Equinoxes happen when the ecliptic and celestial equator intersect. When the sun is moving down from above the celestial equator, crosses it, then moves below it, that point of intersection between the two planes is when the autumnal equinox occurs. This usually happens around the 23rd of September. When the sun moves up from below the celestial equator to above it, the point of intersection between the sun and celestial equator is when vernal equinox occurs. It usually happens around 21st of March. During the equinoxes, all parts of the earth experiences 12 hours of day and night and that is how equinox gets it name as equinox means equal night. At winter solstice (December), the North Pole is inclined directly away from the sun. Three months later, the earth will reach the date point of the March equinox and that the sun's declination will be 0 degree. Three months later, the earth will reach the date point of the summer solstice. At this point it will be at declination -23.5 degree. This cycle will carry on, creating the seasons that we experience on earth

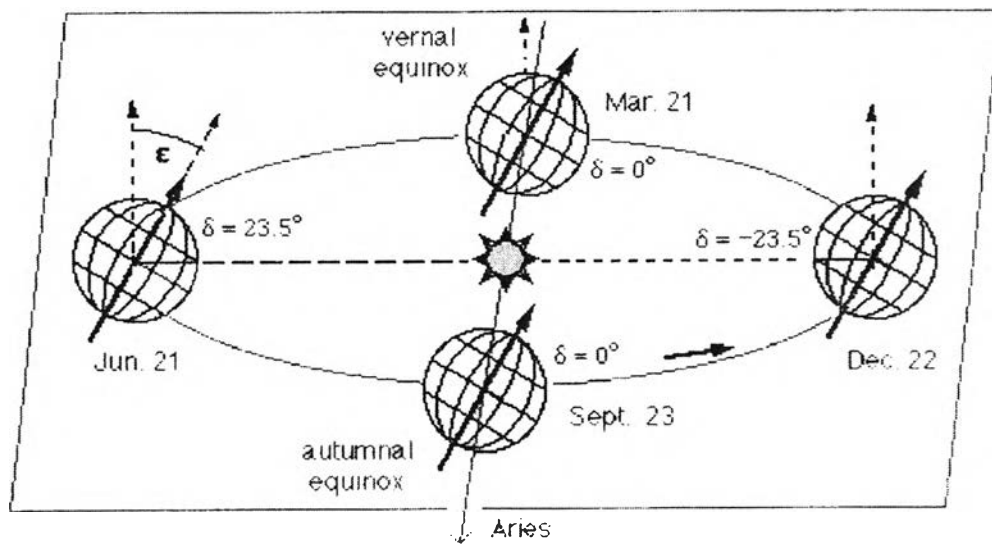

Figure 3.1: Orbit of the earth around the sun. The tilt angle of the earth with respect to the orbit plane is approximately 23.5 degree. The sun crosses the celestial equinox on the 21st March and at autumnal equinox on 23 September. The sun is at its greatest distance from the celestial equator at summer solstice on 21 June and at winter solstice on 22 December.

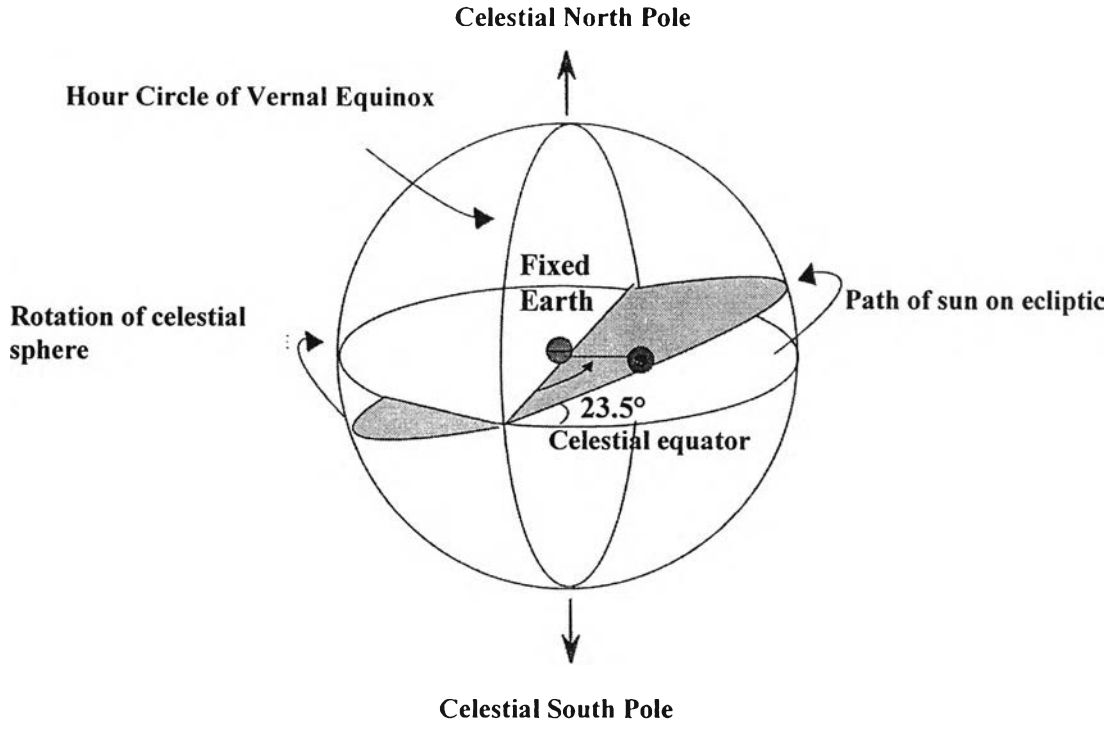

Figure 3.2: The celestial sphere

3.2 The Sun Position – Altitude and Azimuth angle

The sun position on the sky can be specified by altitude and azimuth angles, as shown in Figure 3.3. The solar altitude angle (α) is measured from the horizontal plane upward to the center of the sun. The azimuth angle (ψ) is measured on the horizontal plane between a due south line and the projection of the site-to-sun line on the horizontal plane. The sign convention used for azimuth angle is positive eastward and negative westward. A less convenient angle used by some solar engineers is the zenith angle θ_z, which is the complement of the altitude angle.

Solar altitude and solar azimuth angles are related to the fundamental angular quantities-hour angle, latitude and solar declination- all of which will be described in turn. The three angles are shown in Figure 3.4.

The solar hour angle, H, is equal to 15 degree times the number of hours from local solar noon. Again, value east is positive; value west, negative. The numerical value of 15 degree / hr is based upon the nominal time (24 hr) required for the sun to move around the earth (360 degree) once.

The declination of the sun (δ) is the angle between the sun's rays and the zenith direction at noon on the earth equator as shown in Figure 3.4. Declinations north of the equator (summer in the northern hemisphere) are positive; those south, negative.

The final fundamental angle used to calculate the altitude and azimuth angles is site latitude (ϕ). The latitude may be read from an atlas and is positive north of the equator and negative south.

In order to calculate the solar altitude, the law of cosine for spherical triangles can be applied to triangle NPV in Figure 3.4 with the result

$$\cos(90^\circ - \alpha) = \cos(90^\circ - \phi)\cos(90^\circ - \delta) + \sin(90^\circ - \phi)\sin(90^\circ - \delta)\cos H \qquad (3.1)$$

or in a simplified from of

$$\sin(\alpha) = [\cos(\phi)\cos(\delta)\cos(H)] + [\sin(\phi)\sin(\delta)] . \qquad (3.2)$$

Using a similar technique, the solar azimuth angle can be computed from

$$\cos(\psi) = [\sin(\alpha)\sin(\phi) - \sin(\delta)] / [\cos(\alpha)\cos(\phi)] \qquad (3.3)$$

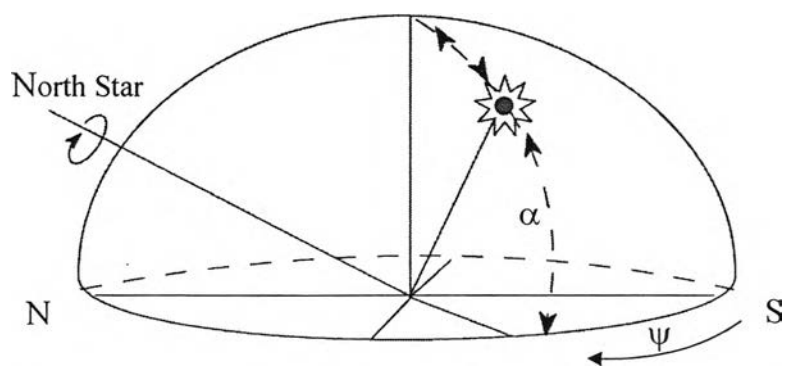

Figure 3.3: Solar altitude (α) and solar azimuth (Ψ) angles

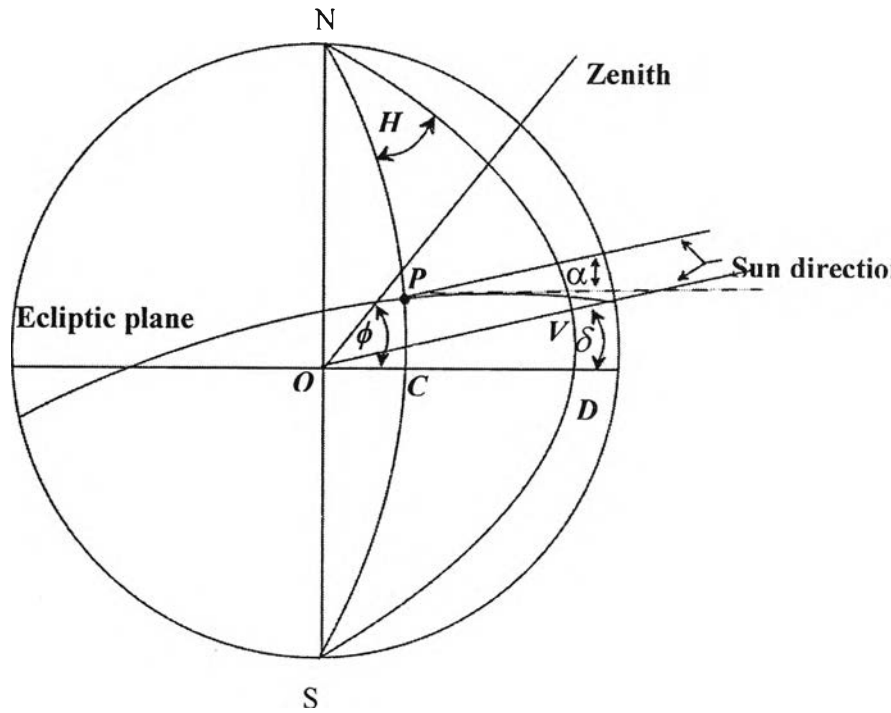

Figure 3.4: Definition of solar-hour angle H (C-N-D), solar declination δ (V-O-D), and latitude ϕ (P-O-C)

3.3 Heliostat field

The central receiver system is one kind solar concentrating system. This system use numbers of heliostats to focus sunlight on to a central receiver situated on a tower. The heliostat field that surrounds the tower is laid out to optimize annual performance of the plant.

A heliostat is the mirror that tracks the sun in such a way that the reflected sunlight always aims at the receiver. The heliostat basically consists of a reflector which can be controlled around two axes to follow the diurnal movement of the sun in order to transfer solar beam to a fixed target. Heliostat is moved around a vertical axis tracking the azimuth of the sun and a second horizontal axis which rotates around the vertical axis to allow tracking the elevation of the sun.

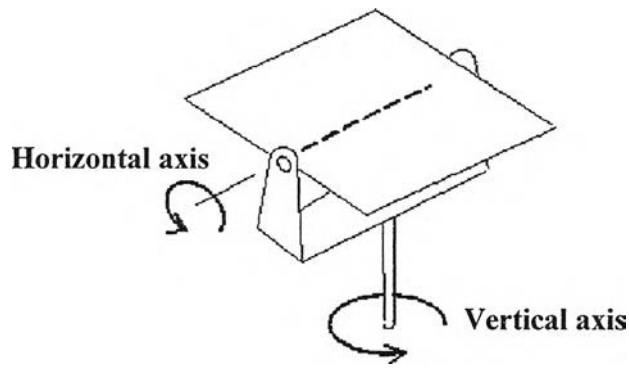

Figure 3.5: Two - axes heliostat

The thermal efficiency of the operation of the central receiver system and its highest achievable temperature depend on several factors, among which are

(1) location of the site,

(2) radiation properties of the heliostat surface and the central receiver,

(3) the orientation and tilt angle of each heliostat and (4) the layout of the heliostat field.

The performance of the heliostat field is defined in term of the optical efficiency; a ratio of the net power intercepted by the receiver to the power incident normally on the field. The optical losses include the cosine effect, shading and blocking losses, imperfect mirror reflectivity and atmospheric attenuation. As heliostats are packed closer together, blocking and shadowing losses increase. The cosine effect depends on both the sun's position and the location of the individual heliostat relative to the receiver. The heliostat is positioned by the tracking mechanism so that its surface normal bisects the angle between the sun's rays and a line from the heliostat to the tower. The effective reflection area of the heliostat is reduced by the cosine of one-half of this angle.

The layout of the heliostat field can be designed using various criteria. The selected criterion is based on that the land area covered by the reflective surface should be maximized. The measure of the land use is the mirror density, defined as net reflecting surface area to land covered area.

The heliostats could be uniformly spaced but with some disadvantages. There might be a shadowing effect, where a reflecting surface of a heliostat comes into the shaded area of another heliostat or blocking effect, where reflected rays by one heliostat could be blocked by the back surface of another heliostat. This effect is more evident at high mirror density.

Analyses are presented to determine the percentage of area of a heliostat that is suffered from shadowing and blocking of another heliostat in a central receiver system. It can be analyzed by the ray-tracing techniques [5]. The analyses are found to depend on the solar time, the day in the year, the location of the site, the height of the central receiver, the relative position of the heliostats, with respect to the tower and with respect to one another, and the dimensions of each heliostat.

Clearly, the heliostats should be carefully distributed in the field so that maximum efficiency is obtained. It is generally best to arrange heliostats in a radial stagger pattern, which is originally proposed by the team of University of Houston [6]. This pattern minimizes land usage as well as shadowing and blocking losses. Heliostats are tightly packed near the tower but must be sufficiently separated to prevent mechanical interference. For heliostats located further from the tower, the spacing between two consecutive rings increases in order to minimize blocking effect.

F.M.F. Siala and M.E. Elayeb used a graphical method to layout the distribution of the heliostats in the field [7]. This method is based on the heliostat radial stagger arrangement as shown in Figure 3.6. In brief, on the horizontal plane, the heliostat is represented by a circle. From top view the diameter of which equals to the heliostat diagonal. On the vertical plane, the diameter of the circle should equal to the height of the heliostat. Heliostats are divided into several groups and each group is divided into many rings. For the same group, any adjacent two rings of heliostats are azimuthally spaced as shown in Figure 3.6 (a). The radius of the second ring in each group is determined from Figure 3.6 (b) where the line $\overline{ab}$ touches both circles. This method is repeated until the mirror density of heliostats decreases significantly. Then a new group of heliostats should be initiated.

In Figure 3.7, we define the directional vector $\hat{S}$ starting from the center of the mirror towards the sun. This vector is independent of heliostat position and can be described in term of directional cosines S_x, S_y, and S_z relative to the tower base. The components of the unit vector for incident ray with respect to the tower base in term of the angles α and ψ are

$$\begin{aligned} S_x &= \cos(\alpha)\cos(\psi), \\ S_y &= \cos(\alpha)\sin(\psi), \\ S_z &= \sin(\psi). \end{aligned} \tag{3.4}$$

Let $\hat{t}$ be a directional vector starting from the center of the mirror toward the receiver surface. The normal vector of the mirror at anytime is therefore

$$\hat{n} = \frac{\hat{t} + \hat{s}}{|\hat{t} + \hat{s}|} \tag{3.5}$$

where $\hat{t}, \hat{n}$, and $\hat{s}$ are on the same plane.

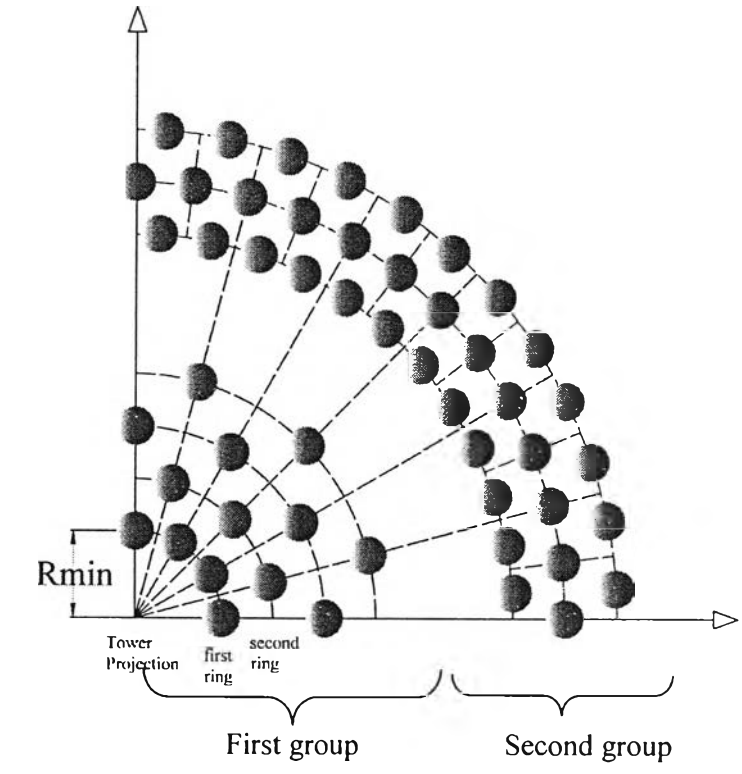

(a) Top view

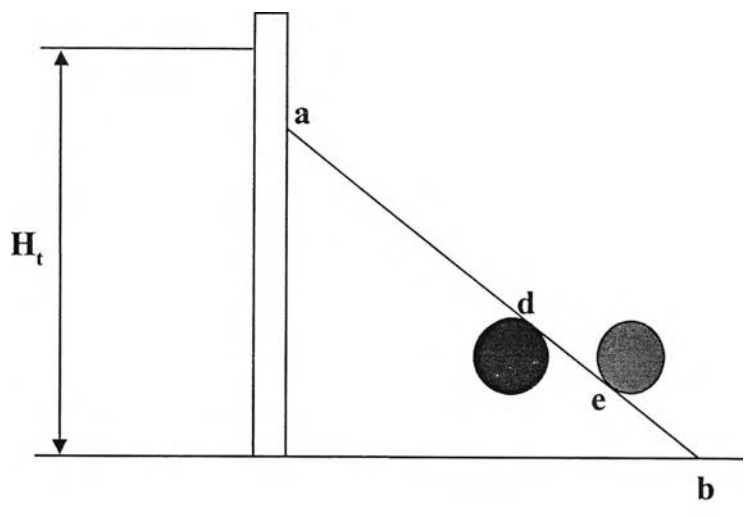

(b) Side view

Figure 3.6: The top view and side view of radial stagger heliostat layout pattern. A heliostat is represented by circle.

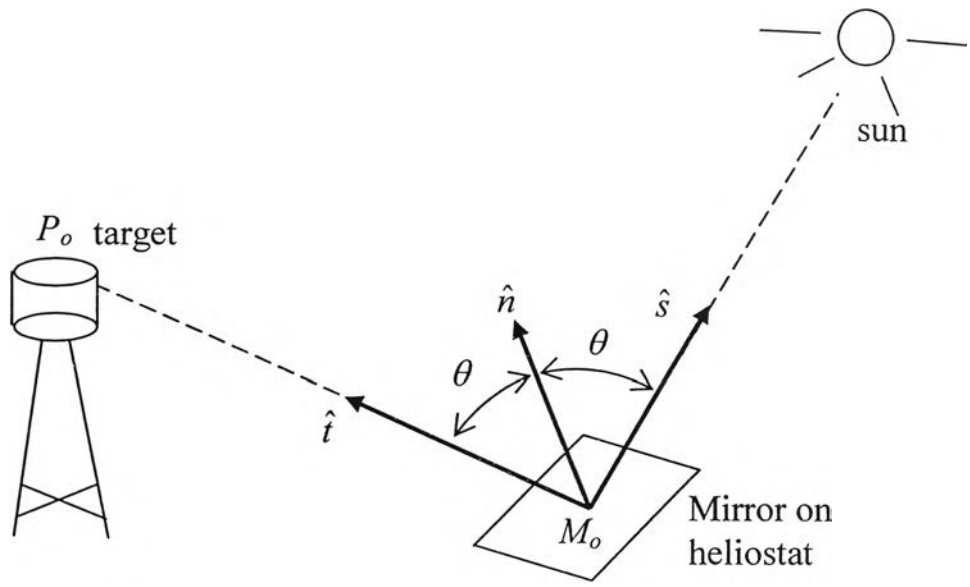

Figure 3.7: Schematic diagram showing how the angular movement of a mirror can direct the sun ray toward the target

3.4 Solar Flux Density Distribution on Image Plane

3.4.1 Geometry of the Coordinate System

For convenience, there are three coordinate systems used in this research (see Figure 3.8)

1. $(\bar{h}_1, \bar{h}_2, \bar{h}_3)$ - coordinate is a heliostat position coordinate system with $\bar{h}_1$ and $\bar{h}_2$ on the horizontal plane and $\bar{h}_3$ in the vertical direction.

2. $(\bar{m}_1, \bar{m}_2, \bar{m}_3)$ - coordinate is used to specify a point position on the mirror surface. $\bar{m}_1$ is always parallel to the ground. $\bar{m}_1$ and $\bar{m}_2$ are on the plane of the mirror and $\bar{m}_3$ is the normal of the mirror.

3. $(\bar{i}_1, \bar{i}_2, \bar{i}_3)$ - coordinate is that of the image plane where $\bar{i}_1$ is always parallel to the ground, $\bar{i}_1$ and $\bar{i}_2$ are on the image plane, and $\bar{i}_3$ points toward the center of the heliostat.

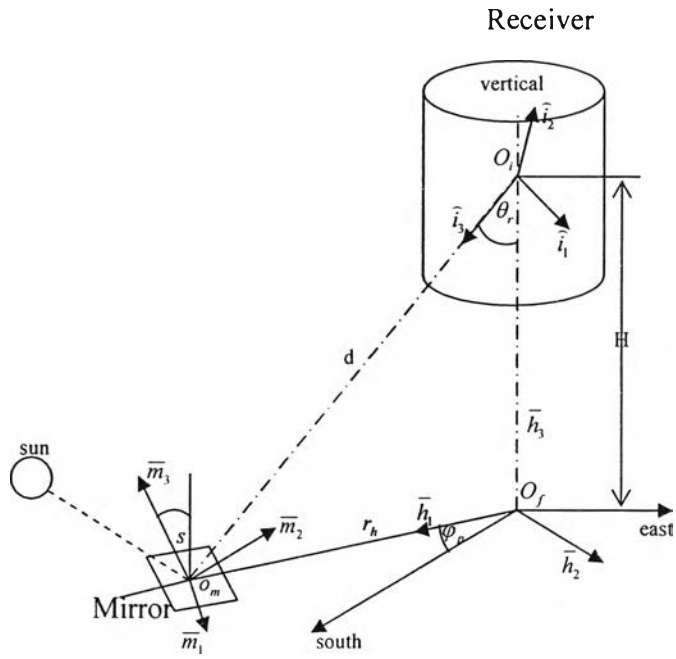

Figure 3.8: The coordinate systems for the heliostat field, mirror, image plane and the receiver plane

3.4.2 The Principal Image of a Heliostat

Consider the flat mirror surface as shown in Figure 3.9(a) with coordinate $\bar{m}_1$ and $\bar{m}_2$. Assuming parallel solar rays and neglecting any error due to the imperfection in the reflecting surface and in the tracking mechanism, the image of the mirror on the image plane would appear as shown in Figure 3.9(b) where points A_i, B_i, C_i, and D_i correspond to the mirror corners A, B, C and D respectively. This image is called the principal image. The principal axes of this image are ξ and η. An angle θ_1 is the anticlockwise angle between the line $O\xi$ and the axis $\bar{i}_1$. The angle θ^* is the

anticlockwise angle between the line $O\eta$ and the axis $O\xi$. The lengths L_H and L_T of the principal image correspond to D_H and D_T of the mirror.

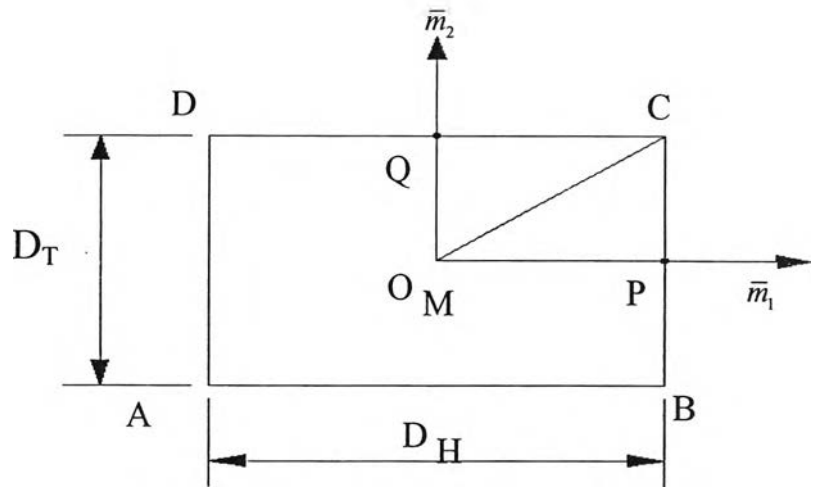

(a) Mirror surface and mirror coordinate

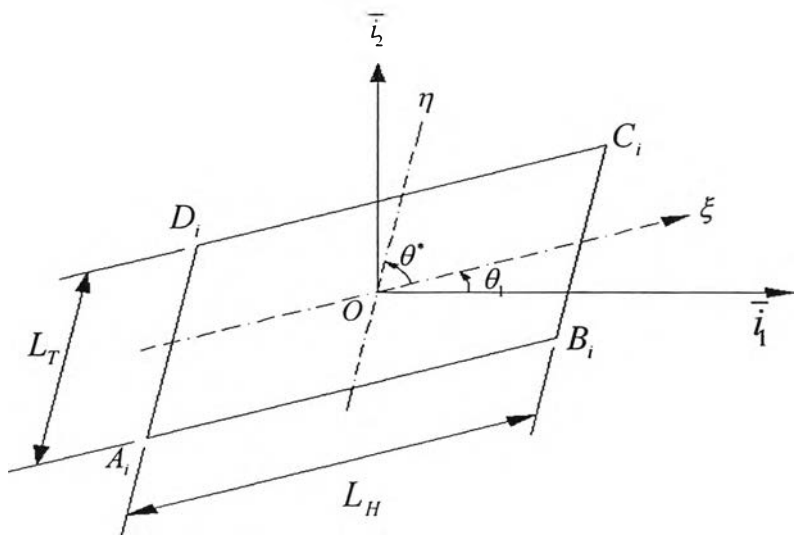

(b) Principal image and image plane coordinate

Figure 3.9: Mirror plane and image plane and their coordinates assuming the sun as a point source

$(\bar{m}_1, \bar{m}_2)$ coordinate can be expressed in term of the (ξ, η) coordinate with the following procedure:

1) Separate coordinate of any point in ξ-η coordinates into two perpendicular components $\xi + \eta\cos\theta^*$ and $\eta\sin\theta^*$.

2) Rotate $\xi + \eta\cos\theta^*$ and $\eta\sin\theta^*$ clock wisely about the $\bar{m}_3$-axis by θ_1 to become $\bar{m}_2$ and $\bar{m}_1$ respectively.

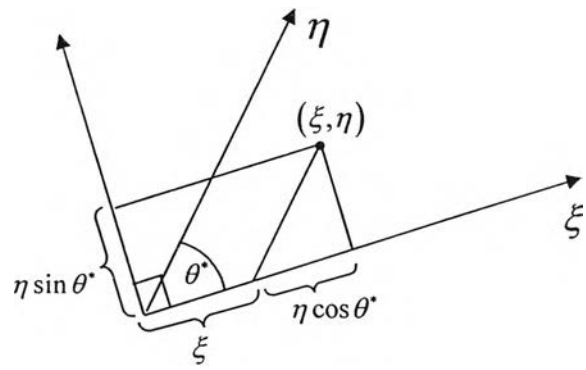

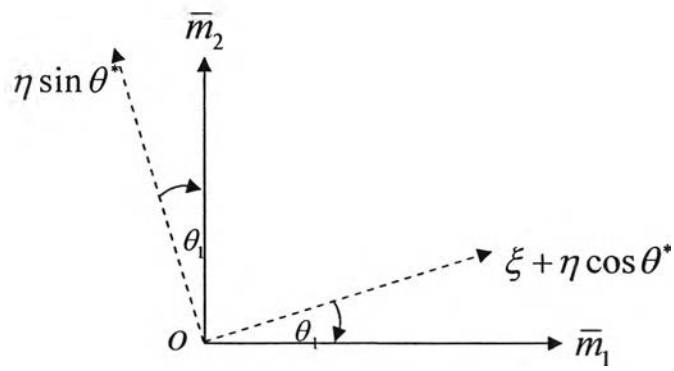

Figure: 3.10: The $(\bar{m}_1, \bar{m}_2)$ coordinate can be expressed in term of the coordinates ξ and η

Those two steps can be described as

$$\begin{bmatrix} \bar{m}_1 \\ \bar{m}_2 \end{bmatrix} = \begin{bmatrix} \cos\theta_1 & -\sin\theta_1 \\ \sin\theta_1 & \cos\theta_1 \end{bmatrix} \begin{bmatrix} 1 & \cos\theta^* \\ 0 & \sin\theta^* \end{bmatrix} \begin{bmatrix} \xi \\ \eta \end{bmatrix}. \tag{3.6}$$

3.4.3 Principal Image Area

In this section, solar flux density distribution on image plane is calculated. First geometry and area of a principal image of each heliostat are calculated by using ray tracing technique. This technique computes the intersection between a ray from heliostat corner and the receiver surface. The analytical form of the equation depends on the shape of receiver. In this work, the receiver is a cylinder. Any ray can be presented in a vector form as

$$\vec{P}(x,y,z) = \vec{E}(x_0,y_0,z_0) + t\hat{R}(x_d,y_d,z_d), \tag{3.7}$$

where $\vec{E}(x_0,y_0,z_0)$ represents the initial position of the reflecting ray. $\hat{R}(x_d,y_d,z_d)$ represents the reflecting ray directional vector from center of mirror to center of cylinder. The variable t indicates how far along the ray the intersection point $\vec{P}(x,y,z)$ is on the cylinder.

The geometry of principal image on the image plane is parallelogram. For a special case where the sun altitude is 90 degrees, the geometry of image is rectangle. The area of this image can be calculated following

$$1/2 \mid (x_1y_2 + x_2y_3 + x_3y_4 + \ldots + x_ny_1) - (y_1x_2 + y_2x_3 + y_3x_4 + \ldots + y_nx_1)\mid, \tag{3.8}$$

where (x_i,y_i) is the vertices of polygon, arranged in a clockwise or anticlockwise manner. If the coordinates are arranged in a clockwise manner, the value within absolute sign is negative. If the coordinates are arranged in a counterclockwise manner, the value within the absolute sign is positive.

3.4.4 The Cone of Reflected Rays

So far, the sun is assumed the perfect point source. In fact, the finite size of the sun makes the reflecting sunlight from any point on the mirror surface belonging to a light cone of solid angle *(s)*

$$S = \pi\alpha_s^2 \tag{3.9}$$

α_s is a solar angle and $\alpha_s \simeq 0.5$ degree [8].

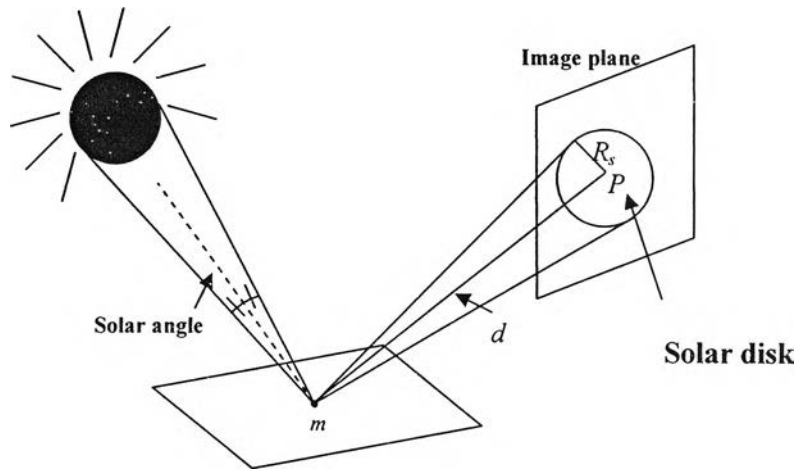

Figure 3.11: The mapping of the sun on image plane due to point *m*

The intersection of the cone with the image plane can be assimilated to a solar disk of center *P*. The radius of solar disk (R_s) depends on the distance *d* between the mirror center and the aiming point at the center of the receiver plane, where

$$R_S = d\tan\alpha_s . \tag{3.10}$$

The distribution of the solar intensity on solar disk is circular, i.e.

$$\begin{aligned} S &= S(r_s), 0 \le r_s \le R_s \\ S &= 0; r_s > R_s \end{aligned} \tag{3.11}$$

The solar intensity $S(\alpha)$ is a function of α. Among several empirical models of $S(\alpha)$ we have selected the one proposed by Walzel et al.[9]

$$S(\alpha) = S_O \left\{ 1 - \lambda \left(\frac{\alpha}{\alpha_S} \right)^4 \right\} \qquad (3.12)$$

where $\lambda = 0.5138$ and $0 \le \alpha \le \alpha_s$. Solar intensity equals to S_O when $\alpha = 0$ and decreases to zero when $\alpha \approx 0.6$ degree.

By definition, the solar intensity $S(\alpha)$ is the rate of energy propagation in a given direction per unit solid angle and per unit area. The solar intensity is related to the solar beam irradiance at normal incidence G_{bn}. From equation (3.12) we can draw the relation between $S_o(W.m^{-2}.sr^{-1})$ and the normal flux density $G_{bn}(W.m^{-2})$ at the consider time

$$G_{bn} = \int_0^{\alpha_s} S(\alpha) \cdot 2\pi \tan(\alpha)(1 + \tan^2 \alpha) d\alpha \,. \qquad (3.13)$$

(see Appendix B for the derivation of equation (3.13))

The terms higher than α_s^3 can be neglected which yields

$$G_{bn} \cong S_0 \pi \alpha_S^{\,2} \left(1 - \frac{\lambda}{3} \right) \qquad (3.14)$$

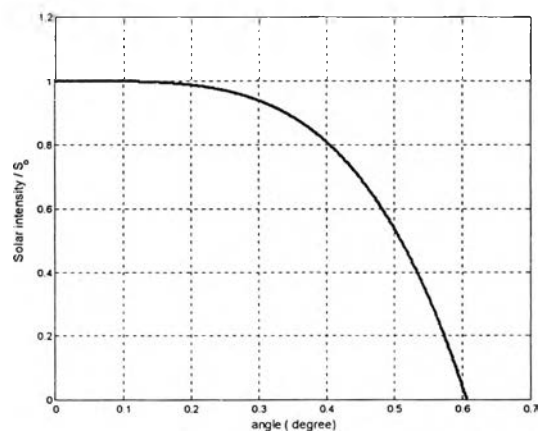

Figure 3.12: Solar intensity

3.4.5 Solar Flux Density Distribution on the Image Plane

A computer simulation of the solar flux density distribution of the central receiver system requires knowledge of the flux density of reflected sunlight due to each heliostat in the field. The problem of calculating the flux density of light reflected by a single heliostat can be formulated in various ways, but each has its limitations. The Monte-Carlo approach represents all of the heliostat behavior but is slow [10]. FLASH is an analytical exact approach for flat polygonal heliostat but it is slow and not application to dished heliostat [11]. Cone optic programs evaluate the flux density by a direct numerical integration of double integral, but method is very slow if accuracy is required [12]. Finally, HOCEF is a two dimensional Hermite polynomial method which is fast but the polynomial approximation breaks down for near heliostat [9].

In our work, the solar flux distribution on a given image plane is calculated by the superposition technique [13]. The concept of this is that an infinitely-small area of a mirror produces a light cone of sunlight. The superposition of this cone from all over area of the mirror produces the flux distribution on the image plane. For each cone, there exists the distribution following equation (3.12).

A point m on the mirror plane causes a pinhole image S of solar disk intercept with principal image P. The solar flux density, F, on the image plane is the convolution of S and P. Following Refs. 9 and11, this could be given as

$$F = S * P \tag{3.15}$$

which is the integration of S over the intersection area between S and P, as shown in Figure 3.13.

The determination of F in the equation (3.15) depends on the geometry of the principal image and the ratio of the radius of the solar disk S to the lengths of the sides of the principal image. In a special coordinate system both S and P could be normalized by the radius of the effective solar disk to give S' and P' ; then

$$F = S' * P' \tag{3.16}$$

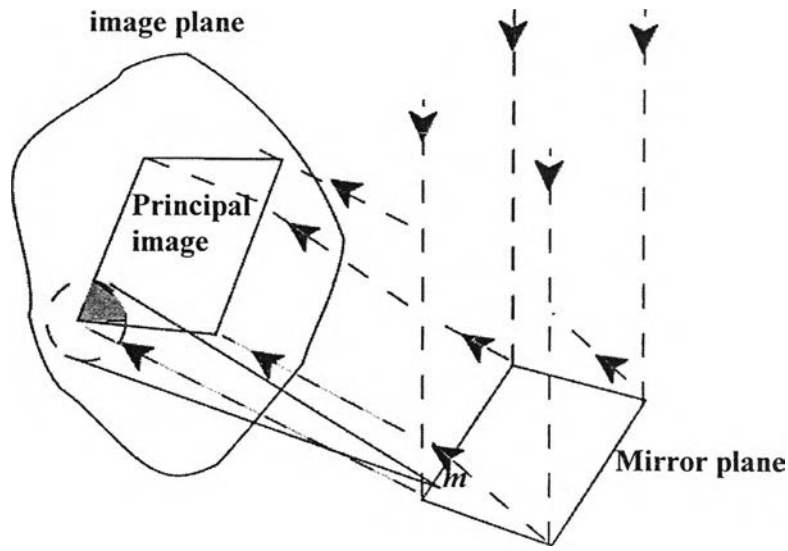

Figure 3.13: The geometry of mirror plane, image plane, and the convolution of solar disk and principal image

Let $P_O(\theta^*)$ be the normalized principal image and with angle θ^* at corner O, the solar flux density distribution F_O is then given as

$$F_O(\theta^*) = S' * P_O(\theta^*) \tag{3.17}$$

For a point O_i on $P_O(\theta^*)$, the flux density $F_O(\theta^*)$ is dependent only on the coordinates (ξ,η) of point O and angle θ^*, as shown in Figure 3.14. For the normalized principal image P' of finite sides L'_H and L'_T and corners A, B, C and D the flux density distribution F then become:

$$F = F_A(\theta^*) + F_C(\theta^*) - F_B(\theta^*) - F_D(\theta^*) \tag{3.18}$$

The above equation is obtained from equation (3.17) by superposition. The distribution F_A, F_B, F_C and F_D are all obtained from F_O after transforming the $\xi - \eta$ coordinate from point O to the points A, B, C and D, respectively.

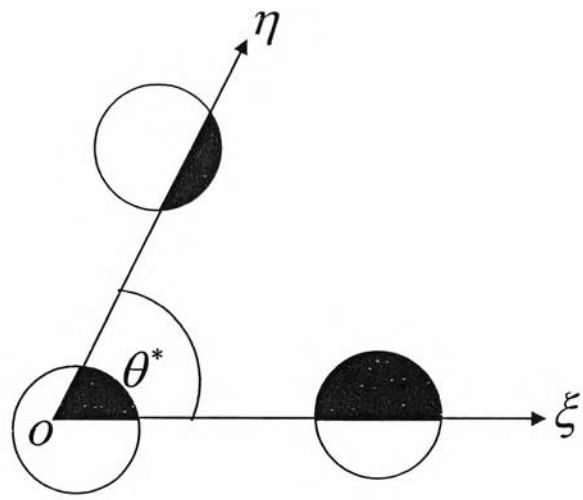

Figure 3.14: Convolution of S' with $P_O(\theta^*)$ to give $F_O(\theta^*)$

Following Ref.14 the convolution of the unit sun disk S' with the principal image of corner O and with infinite lengths of sides is given by

$$F_O(\theta^*,\xi,\eta) = \rho C \iint_a S' d\xi d\eta \tag{3.19}$$

where ρ is the reflectivity of the mirror, C is concentration ratio and F obtained by the integration to be carried out over the intersection area a between S' and P_o of corner at O and the center of S' is at the point (ξ,η).

Equation (3.19) may then be rewritten in the following form:

$$F_0'(\theta^*,\xi,\eta) = \rho C G_{bn} \Phi(\theta^*,\xi^*,\eta^*) \tag{3.20}$$

where Φ is a dimensionless flux distribution function . If S' fall fully inside $P_0(\theta^*)$ and thus $\Phi = 1$. But, S' cannot intersect $P_0(\theta^*)$ and thus $\Phi = 0$.

$$\Phi(\theta^*,\xi^*,\eta^*) = \iint_a \frac{S'}{G_{bn}} d\xi^* d\eta^* \tag{3.21}$$

with:

$$\xi^{\bullet} = |\sin\theta^{\bullet}|\xi \quad ; \quad \eta^{\bullet} = |\sin\theta^{\bullet}|\eta \tag{3.22}$$

Equation (3.18) and (3.20) are combined to give:

$$F = \rho C G_{bn}[\Phi_A + \Phi_C - \Phi_B - \Phi_D] \tag{3.23}$$

3.4.6 The Procedure to Determine the Flux Dimensionless by Superposition Technique.

$\Phi_A, \Phi_C, \Phi_B, \Phi_D$ are the flux dimensionless with the origin of $\xi^{\bullet}$ and $\eta^{\bullet}$ coordinates transferred to the corners *A, B, C* and *D* respectively.

The domain of integration *a* in equation (3.21) is divided into five zones as shown in Figure 3.15. Only zone 1 needs to be determined either numerically or analytically. In zone 2 where $-1 \le \xi^{\bullet} \le 1$, Φ is independent of $\eta^{\bullet}$ and thus it could be obtained directly from zone 1. Similarly, in zone 3, where $-1 \le \eta^{\bullet} \le 1$, Φ is independent of $\xi^{\bullet}$, and it is the same as its value on the edge of zone 1. In zone 4, S' fall fully inside $P_0(\theta^{\bullet})$ and thus $\Phi = 1$. In zone 5, S' cannot intersect $P_0(\theta^{\bullet})$ and thus $\Phi = 0$. The distribution of Φ in zone 1 could then be determined once S' is specified.

From equation (3.21) it is difficult to find limit of integral thus we transfer coordinate $(\xi^{\bullet}, \eta^{\bullet})$ to corner *A, B, C* and *D* respectively. So that limit of integral is zero to infinite. The procedure to determine the solar flux dimensionless on the image plane is as follows:

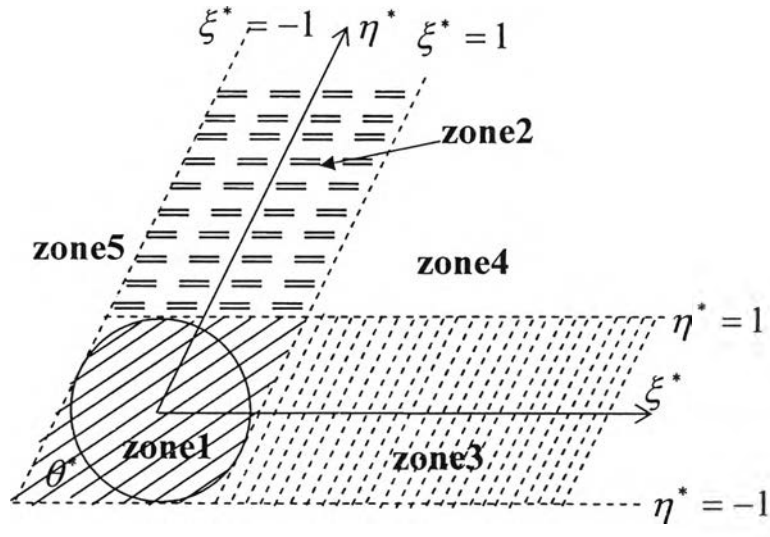

Figure 3.15: Zone of the flux density distribution on the infinite principal image $P_0(\theta^*)$

1. Determine the (ξ^*, η^*) on the image plane which corresponds to $(\bar{m}_1, \bar{m}_2)$, using equation (3.6) and (3.22). In this example, let consider the top-right corner of the mirror.

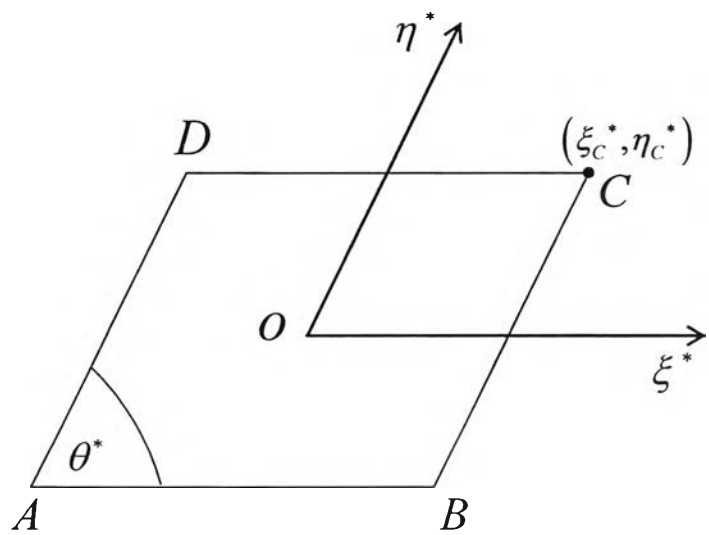

2. Draw a unit solar disk centered at (ξ_c^*, η_c^*).

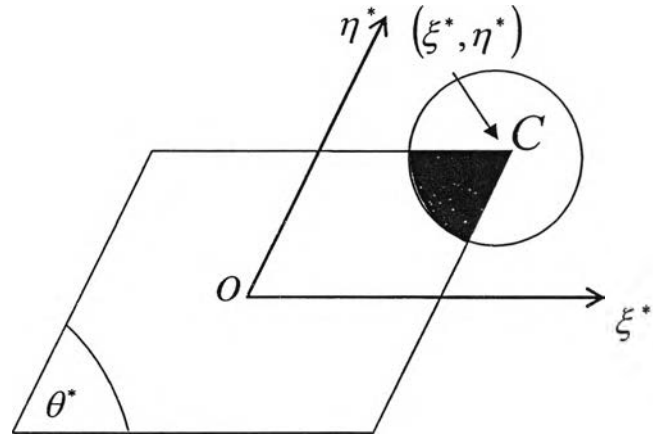

3. Move the origin of coordinate (ξ^*, η^*) to the corner *A*, calculate Φ_A. In this picture, it is $\Phi_A = 1$ because the whole circle is within the 1st quadrant of (ξ^*, η^*) coordinate.

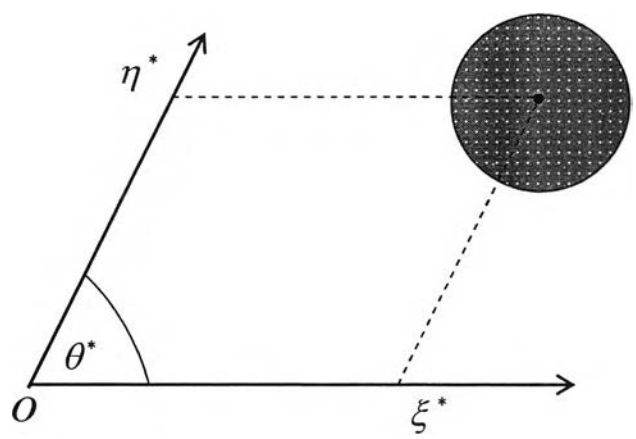

4. Move the origin of coordinate (ξ^*,η^*) to the corner *B*, calculate Φ_B. In this picture, it is $\Phi_B = 0.5$ because the half of circle is within the 1st quadrant of (ξ^*,η^*) coordinate.

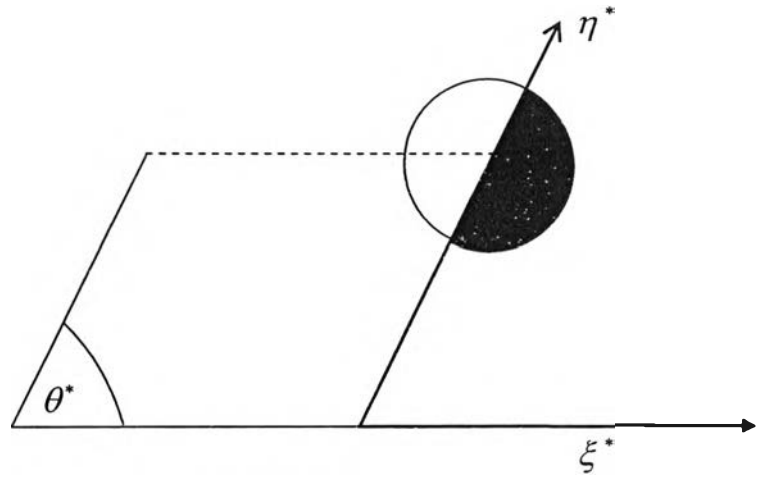

5. Move the origin of coordinate (ξ^*,η^*) to the corner *C*, calculate Φ_C In this picture, it is Φ_C less than 0.5 because the few of circle within the 1st quadrant of (ξ^*,η^*) coordinate.

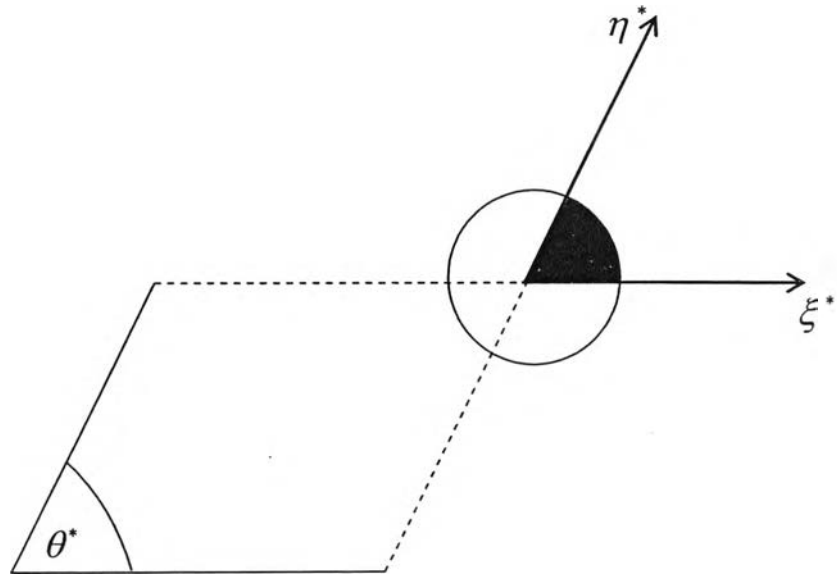

6. Move the origin of coordinate (ξ^*,η^*) to the corner *D*, calculate Φ_D. In this picture, it is $\Phi_D = 0.5$ because the half of circle within the 1st quadrant of (ξ^*,η^*) coordinate.

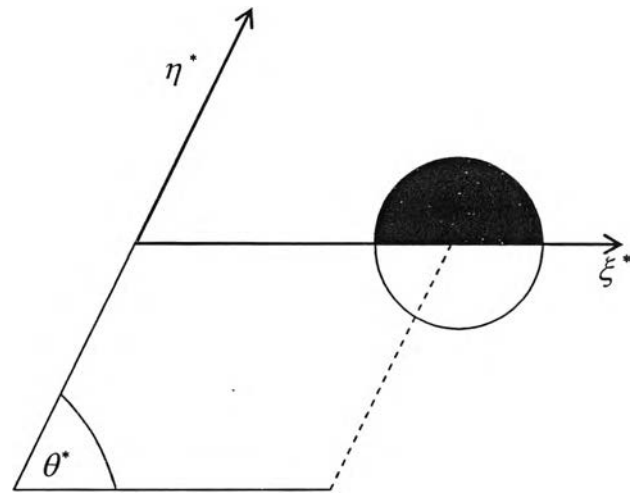

7. The last, calculate Φ for point (ξ^*,η^*) by equation (3.18)

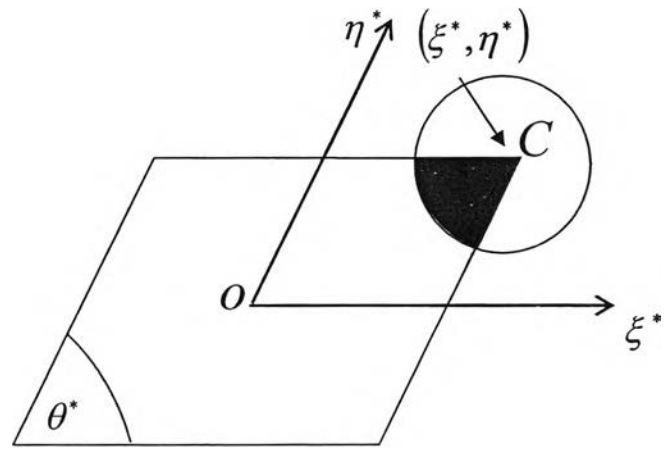

$$\Phi(\xi^*,\eta^*) = \Phi_A - \Phi_B + \Phi_C - \Phi_D \tag{3.24}$$

3.5 Solar Flux Density Distribution on the Cylindrical Receiver Surface

The solar flux density distributions produced on the surface of a central tower receiver by large mirror fields have been determined using the superposition technique. All distributions are transferred from the image plane onto the cylindrical surface via our two-stage projection.

The first projection, we project each point on principal image to a plane that normal vector parallel to radius of cylinder by ray tracing as shown in Figure 3.16. The height of principal image is increased but the width of principal image is the same.

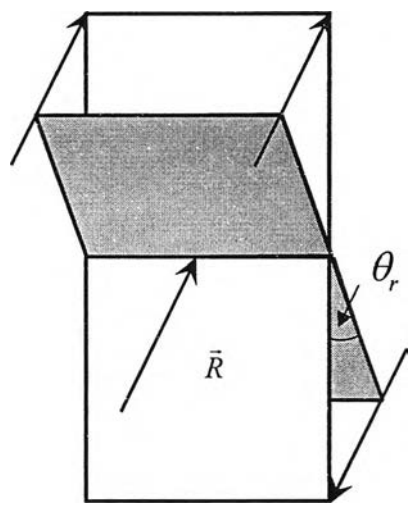

Figure 3.16: The first projection

The second projection, we project each point on that plane from the first projection on to surface of cylinder by ray tracing again. Cylindrical surface is divided to small window, the 1 degree in horizontal and the height in vertical is 1 cm. Each point of principal image on image plane is projected onto cylindrical surface. If it is a decimal, it is rounded to the nearest integers. θ_R is surface angle, measured from south in eastward direction.

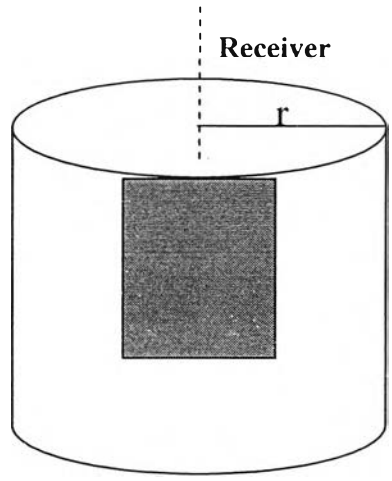

(a) Side view

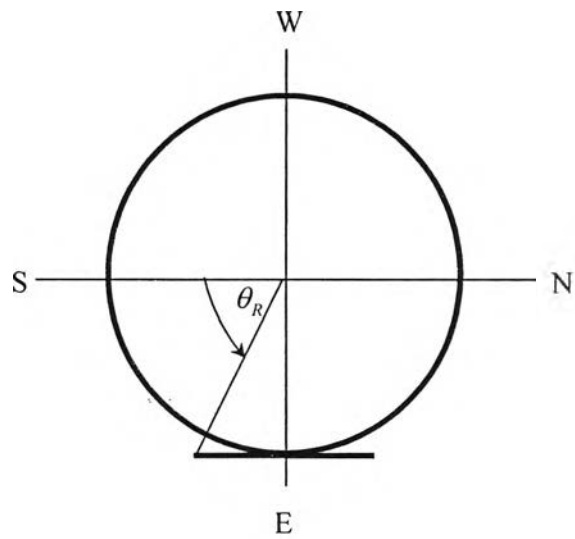

(b) Top view

Figure 3.17: Projection on to surface of cylinder

The flux density Γ at point (x_R, y_R) on the receiver plane is given in terms of flux density function F on the image plane by the following relation

$$\Gamma(x_R, y_R) = \sin\theta_r F(\xi^*, \eta^*) \tag{3.25}$$

where θ_r is tower altitude (see Figure 3.16)

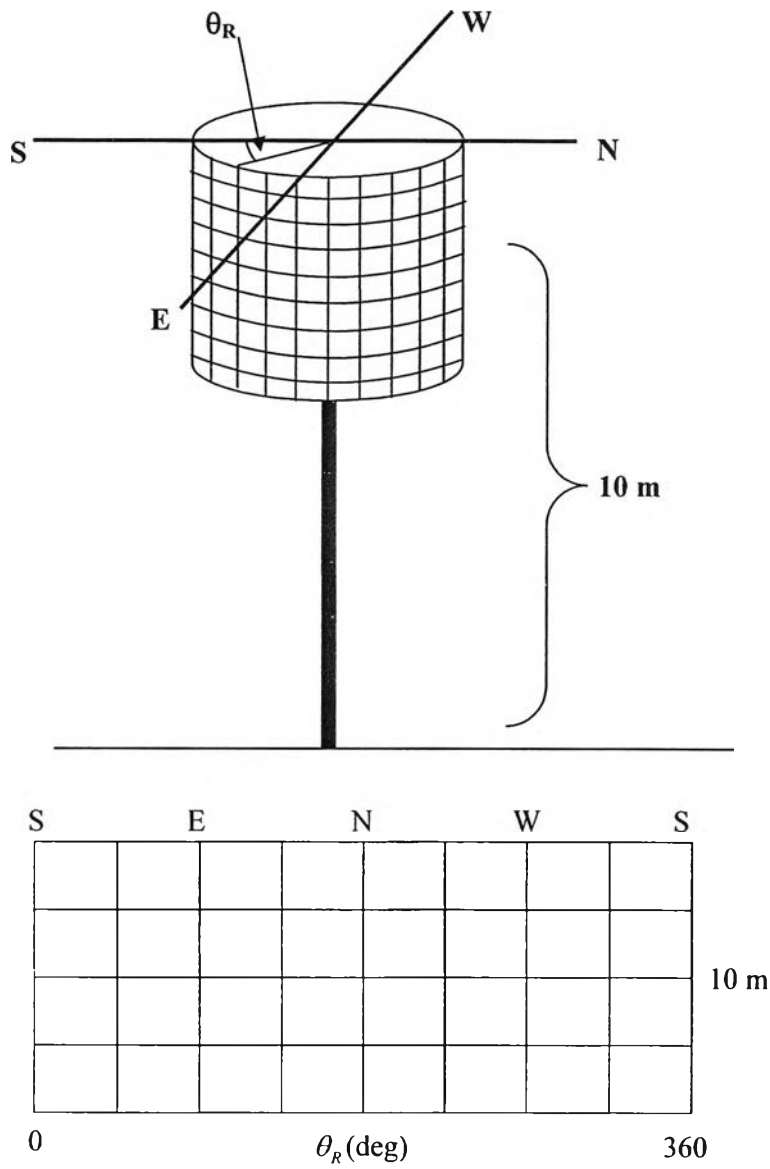

Figure 3.18: Cylindrical surface is divided to small window